

A targeted search for FRB counterparts with *Konus-Wind*

A. Ridnaia,¹★ D. Frederiks,¹ and D. Svinkin¹

¹*Ioffe institute, Politekhnicheskaya 26, St. Petersburg 194021, Russia*

Accepted 2023 November 15. Received 2023 November 13; in original form 2023 September 29

ABSTRACT

We present results of the search for hard X-ray/soft γ -ray emission in coincidence with publicly reported (via Transient Name Server, TNS †) fast radio bursts (FRBs). The search was carried out using continuous *Konus-Wind* data with 2.944 s time resolution. We perform a targeted search for each individual burst from 581 FRBs, along with a stacking analysis of the bursts from 8 repeating sources in our sample and a separate stacking analysis of the bursts from the non-repeating FRBs. We find no significant associations in either case. We report upper bounds on the hard X-ray (20 - 1500 keV) flux assuming four spectral models, which generally describe spectra of short and long GRBs, magnetar giant flares, and the short burst, coincident with FRB 200428 from a Galactic magnetar. Depending on the spectral model, our upper bounds are in the range of $(0.1 - 2) \times 10^{-6}$ erg cm⁻². For 18 FRBs with known distances we present upper bounds on the isotropic equivalent energy release and peak luminosity. For the nearest FRB 200120E, we derive the most stringent upper bounds of $E_{\text{iso}} \leq 2.0 \times 10^{44}$ erg and $L_{\text{iso}} \leq 1.2 \times 10^{44}$ erg s⁻¹. Furthermore, we report lower bounds on radio-to-gamma-ray fluence ratio $E_{\text{radio}}/E_{\text{iso}} \geq 10^{-11} - 10^{-9}$ and compare our results with previously reported searches and theoretical predictions for high-energy counterparts to FRBs.

Key words: gamma-rays: stars – transients: fast radio bursts – stars: magnetars

1 INTRODUCTION

Fast radio bursts (FRBs) are exceptionally bright (\sim Jy), short-duration (\sim ms) radio transients, discovered serendipitously in 2007 (Lorimer et al. 2007). The dispersion measures (DM) of observed FRBs are well in excess of the expected Milky Way contribution, which implies they are originating from extragalactic distances (see, e.g. Cordes & Chatterjee (2019); Petroff et al. (2022), for a review). Over 600 unique sources have been reported thus far by different radio telescopes (see Table 1), including 492 sources detected by the Canadian Hydrogen Intensity Mapping Experiment Fast Radio Burst (CHIME/FRB) Project (CHIME/FRB Collaboration et al. 2021). Among them, only 18 (Chatterjee et al. 2017; Ravi et al. 2019; Bhandari et al. 2020, 2022) FRBs have been localized with enough (sub-arcsecond to arcsecond) precision to identify their host galaxies and redshifts, which confirms extragalactic origins and reveals a wide range of galaxy types and local environments surrounding the FRBs (Heintz et al. 2020). More than half of these localizations have been provided by the Australian Square Kilometre Array Pathfinder (ASKAP; Macquart et al. 2010). While most FRBs are only seen once (“one-offs”), a small fraction (\sim 4 %) of them have been found to produce multiple bursts (“repeaters”) (Spitler et al. 2016; CHIME/FRB Collaboration et al. 2021; Fonseca et al. 2020; Andersen et al. 2023). It remains an open question whether all FRBs repeat, and whether multiple progenitor populations of FRBs exist.

Until now, no clear physical picture of either the central-engine that produce a FRB or the mechanism by which the emission is gen-

erated has emerged. A wide range of models have been proposed, none of which is able to explain alone the variety of observed events (see Platts et al. 2019 for a review). The most debated progenitor models include magnetars as their central-engines, with the FRB emission originating inside or outside of the magnetosphere (Popov & Postnov 2010; Zhang 2020; Kumar et al. 2017; Katz 2014; Lyubarsky 2014; Metzger et al. 2019; Beloborodov 2017, 2020). The recent discovery of a FRB-like event from the Galactic magnetar SGR 1935+2154 (FRB 200428; Bochenek et al. 2020; CHIME/FRB Collaboration et al. 2020) strongly suggests that at least some fraction of FRBs may originate from magnetars. The bright radio burst FRB 200428 was accompanied by the simultaneous emission of hard X-rays with properties similar to those of the short bursts typical of Galactic magnetars (Mereghetti et al. 2020; Ridnaia et al. 2021; Li et al. 2021; Tavani et al. 2021), except for the peculiarly hard energy spectrum (Ridnaia et al. 2021). A couple more coincident radio and high energy events were detected from the same source (Dong & Chime/Frb Collaboration 2022; Wang et al. 2022; Frederiks et al. 2022; Maan et al. 2022; Huang et al. 2022; Li et al. 2022), characterized by much fainter radio emission and longer duration than FRB 200428, and softer X-ray spectra typical of magnetar bursts.

To date, there is no other confirmed multi-wavelength or multi-messenger transient being associated with any FRB. The presence or absence of a simultaneous or delayed emission corresponding to FRBs in different wavebands would be essential to constrain the emission mechanisms and to identify the FRB progenitor(s). In the last years, many multi-wavelength searches for FRB counterparts have been carried out at all wavelengths with no confirmed results (see, e.g., Nicastro et al. 2021 for a review). In high-energy domain, a number of systematic searches has been made by using archival data of

★ E-mail: ridnaia@mail.ioffe.ru

† Transient Name Server (TNS), <http://www.wis-tns.org/>

Fermi (GBM, Martone et al. 2019; LAT, Principe et al. 2023), *INTEGRAL* (IBIS-ISGRI, Mereghetti et al. 2021), *AstroSat* (CZTI, Anumarlapudi et al. 2020), *Insight-HXMT* (HE, Guidorzi et al. 2020), *AGILE* (MCAL, GRID; Verrecchia et al. 2021), and data of multi-wavelength campaigns involving multiple instruments (Cunningham et al. 2019; Trudu et al. 2023). However, most of these studies were based on small FRB samples (less than 50 sources) or only focused on certain objects.

In this work, taking the advantages of the huge increase in the number of detected FRBs and continuous full-sky observations covering the entire current era of FRBs, performed by the *Konus-Wind* γ -ray spectrometer (KW), we carry out a targeted search for possible hard X-ray/soft γ -ray counterparts to over 700 publicly reported bursts from repeating and non-repeating FRBs in KW archival data. The structure of this paper is the following. In Section 2 we provide the FRB sample used in the search and briefly describe our search methodology and upper bound calculations. In Section 3 we present our results, to then discuss it and provide our summary and future prospects in Section 4.

2 DATA AND ANALYSIS

2.1 FRB sample

For our analysis we extract all publicly reported FRBs from TNS (799 events, accessed on 2022 April 27). Six events had to be discarded due to incomplete event information, such as FRB coordinates or burst time arrival, and 25 events due to gaps in the KW data at the time of interest. In addition, we decided to exclude 14 repeating sources, which have less than six bursts per source and have no accurate localization. Thus, the FRB sample used in our analysis consists of 721 events detected with 14 radio telescope facilities (see Table 1) between 2001 January 25 and 2022 January 5. This includes 573 thus far one-off FRBs and 148 bursts from eight repeating sources: FRB 121102A, FRB 180814A, FRB 180916B, FRB 181030A, FRB 190303A, FRB 190711A, FRB 200120E, FRB 201124A. Full list of FRB events considered in the analysis and their measured parameters are available at the webpage¹. Figure 1 shows the dispersion measure distribution of the selected FRBs. To derive upper bounds on the radio-to-high-energy fluence ratio, we use fluence measurements from the first CHIME/FRB catalog (CHIME/FRB Collaboration et al. 2021).

2.2 Konus-Wind analysis

Konus-Wind is a gamma-ray spectrometer which has been successfully operating since November 1994 (Aptekar et al. 1995). KW orbit is far from the Earth magnetosphere (since 2004 at distance of ~ 5 light seconds) that enables nearly uninterrupted observations of entire sky under very stable background. The continuous KW waiting-mode data consist of count rates in $\sim 20 - 80$ keV (G1), $\sim 80 - 320$ keV (G2), and $\sim 320 - 1300$ keV (G3) bands with temporal resolution of 2.944 s. These data are a valuable resource for various studies on hard X-ray/soft gamma-ray transients (Kozlova et al. 2019; Ridnaia et al. 2020).

To search for FRB counterparts, we first estimate the burst arrival time T_0 at the KW position for each FRB. For this, we make two time corrections: a frequency-dependent time delay due to dispersion of the radio frequency with respect to soft γ -rays (infinite frequency)

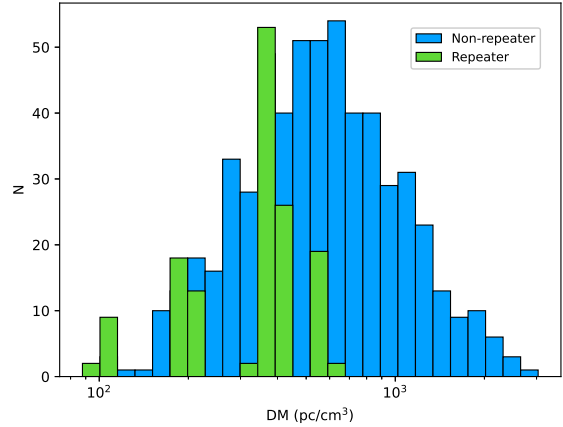


Figure 1. Dispersion measure (DM) distribution of our selected sample of 581 FRBs: 573 “one-off” events and 148 bursts from 8 repeating sources. 18 FRB sources that have been associated with a host galaxies, have a luminosity distances range from 3.6 Mpc to 4 Gpc.

and a propagation time delay between KW and the telescope site. The combined corrections range from few milliseconds to hundreds of seconds, with a mean (median) value of 9.2 (4.9) s. We then search for significant ($> 5\sigma$) excess over background during the 400 s time interval centered on T_0 . While the search interval length of 400 s is chosen arbitrarily, we were motivated by the discovery of the Galactic FRB 200428 accompanied by the simultaneous emission of hard X-rays and by theoretical predictions of very weak high-energy emission on time scales of (at most) minutes after the radio signal (Lu et al. 2020; Metzger et al. 2019). The search is performed in six energy channel combinations (G1, G2, G3, G1+G2, G2+G3 and G1+G2+G3), on temporal scales from 2.944 s to 100 s, similar to Svinkin et al. (2019). The linear background approximation is estimated using two time intervals, before ($T_0 - 1000$ s, $T_0 - 250$ s) and after ($T_0 + 250$ s, $T_0 + 1000$ s) the search interval.

2.2.1 Upper bound on the peak flux and fluence

In the case of non-detection of a significant counterpart in the KW data, we estimate upper bounds on its peak energy flux and energy fluence using four template spectral models, which represent typical short and long GRBs (Svinkin et al. 2016; Tsvetkova et al. 2017), huge initial pulses of magnetar giant flares (MGFs; Svinkin et al. 2021), and the Galactic SGR/FRB 200428 event (Ridnaia et al. 2021). These models are characterized by the Band function (Band et al. 1993) or an exponentially cut off power law (CPL), with the parameters listed in Table 2.

In this work we use upper bound on the gamma-ray flux defined as the upper edge of a (frequentist) confidence interval for the flux of the source, according to Kashyap et al. (2010). To estimate an upper bound C_{ub} on the source counts in a particular KW light curve, measured in the energy band ΔE , we use the bin with the maximum count rate, for which C_{max} is the observed number of counts, C_{bg} is the estimated number of background counts, and σ_{bg} is the error of the background estimation. We define C_{ub} (corresponding to the confidence level CL, hereafter CL=0.9) so that the probability to observe $C > C_{max}$, assuming that the counts have Gaussian distribution with $\mu = \sigma^2 = (C_{ub} + C_{bg} + \sigma_{bg}^2)$, equals CL (see Figure 2). We find

¹ <http://www.ioffe.ru/LEA/FRB/>

Table 1. List of radio telescope facilities with number of detected FRBs included in our sample.

Facility	FRBs	Frequency range (GHz)	Location
Canadian Hydrogen Intensity Mapping Experiment (CHIME) ¹	566	0.4 – 0.8	Canada
Australian Square Kilometre Array Pathfinder (ASKAP) ²	47	0.7 – 1.8	Australia
National Astronomy and Ionosphere Center, NAIC (Arecibo) ³	12	0.1 – 11	Puerto Rico
Parkes Observatory ⁴	33	0.6 – 26	Australia
Molonglo Observatory Synthesis Telescope (MOST) ⁵	17	0.6 – 1.2	Australia
Robert C. Byrd Green Bank Telescope (GBT) ⁶	15	0.3 – 110	USA
Deep Synoptic Array-110 (DSA-110) ⁷	1	1.3 – 1.5	USA
Effelsberg 100-m Radio Telescope ⁸	4	0.4 – 95	Germany
Five-hundred-meter Aperture Spherical radio Telescope (FAST) ⁹	2	0.1 – 3	China
Giant Metrewave Radio Telescope (GMRT) ¹⁰	4	0.2 – 1.4	India
Large Phased Array (LPA) ¹¹	10	0.109 – 0.111	Russia
Sardinia Radio Telescope (SRT) ¹²	3	0.3 – 116	Italy
Very Large Array (VLA) ¹³	4	0.1 – 50	USA
Westerbork Synthesis Radio Telescope (WSRT) ¹⁴	3	0.1 – 8.3	Netherlands

¹ CHIME/FRB Collaboration et al. (2018) ² Hotan et al. (2021) ³ Cordes et al. (2006) ⁴ Staveley-Smith et al. (1996) ⁵ Mills (1981); Robertson (1991) ⁶ Prestage et al. (2009) ⁷ Ravi & DSA-110 Collaboration (2023) ⁸ Wielebinski et al. (2011) ⁹ Nan et al. (2011) ¹⁰ Swarup et al. (1991) ¹¹ Tyul'bashev et al. (2022) ¹² Prandoni et al. (2017) ¹³ Perley et al. (2011) ¹⁴ Oosterloo et al. (2009)

Table 2. The four source spectrum models used in upper bound calculations.

Description	Model	Parameters		
		α	β	E_p (keV)
Typical long GRB	Band	-1.0	-2.5	300
Typical short GRB	CPL	-0.5	...	500
MGF (GRB 200415A)	CPL	-0.6	...	1190
SGR/FRB 200428	CPL	-0.72	...	85

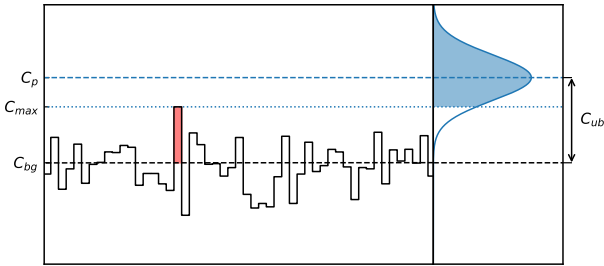


Figure 2. Upper bound calculation. For the bin with the maximum observed count rate C_{\max} (red) we estimate the background count rate C_{bg} (the dashed line). We define upper bound on the source counts C_{ub} (corresponding to the 90 % confidence level) so that the probability to observe $C > C_{\max}$, assuming that the counts have Gaussian distribution with $\mu = \sigma^2 = (C_{\text{bg}} + C_{\text{ub}})$, equals 0.9.

that the last term σ_{bg}^2 contribute less than a percent to the σ^2 , and therefore can be omitted from our calculations.

The upper bound on the source counts then can be converted into a fluence (peak flux) upper bound in the standard energy range (20 – 1500 keV) by using the count-to-energy conversion factor k dependent on ΔE , the template spectrum, the FRB sky location (the angle of incidence), and the corresponding KW detector response. The maximum value of kC_{ub} or $kC_{\text{ub}}/2.944$ s is adopted as the upper bound on the corresponding short (< 2.944 s) event energy fluence or the long event peak energy flux, respectively.

2.2.2 Stacking analysis

Current theories make widely varying predictions about FRB high-energy counterparts, with expected emission being faint (below the threshold sensitivity of the present telescopes) in most of the models (see e.g. Chen et al. 2020). Assuming that parameters determining the hard X-ray/soft γ -ray emission have the same values for all the FRBs, we can employ the stacking analysis. The stacking analysis is a powerful technique that makes it possible to detect sources below the detection threshold. It brings down the statistical noise by combining the signal of many individually undetected sources.

We perform a stacking analysis of the KW data by summing up the background subtracted count rates of the individual event light curves, centered on T_0 and then divided by the number of the summed events. To calculate upper bounds for the resulted light curve we use a similar procedure as described in 2.2.1, except estimating an upper bound R_{ub} on rates instead of C_{ub} on counts. Two sets of upper bounds were computed: one based on the bin with the maximum count rate (assuming that all FRB events have the same large (> 3 s) time delay between FRB and its high-energy counterpart) and the other, on the bin comprising T_0 (the non-delayed case).

We carry out a stacking analysis of the bursts from each repeating source in our sample and a separate stacking analysis of the bursts from the non-repeating FRBs.

3 RESULTS

3.1 Candidate transients

Our search resulted in two candidate transient events, coincident in time with FRB 160206A and FRB 171019A (see Figure 3). The first one turns out to be a GRB 160206B, which was also detected and localized by *Fermi*-GBM (trigger 476446756/bn160206430). The GRB localization is inconsistent with the FRB position, which lies far outside the 3σ GBM localization region.

In the second case, a KW ecliptic latitude response (Svinkin et al. 2022) for the KW-detected transient is inconsistent with the position of FRB 171019A. Moreover, the FRB position is outside Earth-occulted part of the sky for *Swift* and the source is located right at the edge of the BAT coded field of view, and so a FRB-related GRB

Table 3. Upper bounds on the 20–1500 keV fluence (peak flux).

Spectral template	Upper bounds range (10^{-7} erg cm $^{-2}$)
Typical long GRB*	1 – 4
Typical short GRB	5 – 10
MGF, GRB 200415A	9 – 20
SGR/FRB 200428	1 – 7

* For the long burst template, we provide upper bounds on the peak flux in units of 10^{-7} erg cm $^{-2}$ s $^{-1}$.

might be captured by BAT as a count rate excess. We examine BAT data around the time of FRB 171019A and the KW transient² and find no significant count rate increase at 5σ level. This, together with the shape of the KW light curve and its detectors’ response hints towards this transient being an accidentally coincident GRB.

Thus, we conclude that both candidate transients found in our search are physically unrelated to the FRBs. Based on the continuous KW observations between November 1994 and August 2017 (Kozlova et al. 2019) we estimate an average KW GRB detection rate to ~ 0.8 GRB per day. Assuming this rate, an expected number of GRBs detected by KW during the total exposure time of our search (~ 3.25 days) is 2^{+3}_{-2} (95% conf.), which is consistent with the number of the observed events.

3.2 Upper Bounds

Our search did not reveal any significant hard X-ray/soft γ -ray emission associated with the 721 FRB events reported through the TNS and detected between 2001 January 25 and 2022 January 5. Following the procedure of Section 2 we have set upper bounds, that are presented in Table 3. The stacked data analysis allows us to set a factor of 20 (25 in the case of upper bounds based on the bin comprising T_0) on average more stringent than individual upper bounds. Figure 4 summarises the results.

For the FRBs with measured redshifts we estimate upper bounds on the total isotropic-equivalent energy release E_{iso} and peak luminosity L_{iso} (see Table 4). While we calculate these upper bounds for each of the four spectral templates, the bounds listed in Table 4 are given on E_{iso} for short GRBs template and on L_{iso} for long GRBs. On average, upper bounds for MGF spectral template results in a factor of two less stringent values and in a factor of two and a half more stringent values for SGR/FRB 200428 template. The upper bounds derived from the stacked data analysis are reported for the repeating FRBs (the upper bounds computed using T_0 bin are given in parenthesis).

Using the derived fluence/peak flux upper bounds and the available radio fluences from the first CHIME/FRB catalog, we calculate the lower bounds on radio-to-gamma-ray fluence ratio η_{FRB} . The provided radio fluences are lower bounds due to the telescope sensitivity at the centre of the field of view is assumed (CHIME/FRB Collaboration et al. 2021). We show the distribution of these ratios in Figure 5 for the repeating and non-repeating FRBs from the joint TNS and CHIME/FRB sample.

Table 4. Upper bounds on the total isotropic equivalent energy release (short GRBs template) and peak luminosity (long GRBs template) for FRBs with measured redshifts. The upper bounds derived from the stacked data analysis are reported for the repeating FRBs.

FRB	Repeating	Host redshift	E_{iso} (10^{49} erg)	L_{iso} (10^{49} erg/s)
180924B	N	0.3212 ^b	21.76	7.44
181112A	N	0.4755 ^c	38.44	15.05
190102C	N	0.2913 ^b	12.21	4.32
190523A	N	0.6600 ^b	66.64	36.54
190608B	N	0.1178 ^b	2.74	1.07
190611B	N	0.3778 ^b	28.17	9.80
190614D	N	0.60 ^d	65.34	30.12
190714A	N	0.2365 ^b	13.05	5.23
191001A	N	0.2340 ^b	8.40	3.29
191228A	N	0.2432 ^b	14.38	5.67
200430A	N	0.1608 ^b	3.92	1.54
200906A	N	0.3688 ^b	24.65	10.61
121102A	Y	0.1927 ^b	1.58 (0.38)	0.64 (0.16)
180916B	Y	0.0337 ^b	0.02 (0.001)	67.19 (4.67) $\times 10^{-4}$
181030A	Y	0.0039 ^e	6.51(1.11) $\times 10^{-4}$	1.96 (0.34) $\times 10^{-4}$
190711A	Y	0.5220 ^b	28.31 (6.43)	14.59 (2.53)
200120E ^a	Y	(3.6 Mpc) ^f	1.96 (0.38) $\times 10^{-5}$	1.18 (0.27) $\times 10^{-5}$
201124A	Y	0.0979 ^b	0.32 (0.23)	0.12 (0.08)

^a FRB source at a distance of 3.6 Mpc with a formally negative redshift

^b Bhandari et al. (2022) ^c Prochaska et al. (2019) ^d Law et al. (2020)

^e Bhardwaj et al. (2021) ^f Kirsten et al. (2022)

4 DISCUSSION AND CONCLUSIONS

Our results, derived with one of the largest FRB sample used so far, are consistent with that found from previous studies. Cunningham et al. (2019) searched for high-energy counterparts to 23 FRBs in GBM, LAT, and BAT data and found $\eta_{\text{FRB}} \geq 10^5 - 10^7$ Jy ms erg $^{-1}$ cm 2 , which is comparable with the derived in this paper. A search for long-duration (1 to 200 s) γ -ray emission coincident with FRBs was carried out by Martone et al. (2019) in cumulative GBM light curves. They obtained a deep upper limit $\eta_{\text{FRB}} > 10^8$ Jy ms erg $^{-1}$ cm 2 . Both primary classes of FRB models (magnetospheric and maser-shock models) predict prompt high-energy counterparts and specify the ratio between the energy emitted by the counterpart and by the FRB itself (Metzger et al. 2019; Cooper & Wijers 2021; Yang & Zhang 2021). In order to compare our results with theoretical predictions, we have set limits on the radio-to-gamma-ray fluence ratio in dimensionless units. Assuming radio fluence and frequency bandwidth values from the literature (see Table 5) for 12 non-repeating FRBs with known distances we found $E_{\text{radio}}/E_{\text{iso}} \geq 10^{-11} - 10^{-9}$. Although the timescales and energy ranges are not identical to our analysis, this is consistent with the ratios obtained over different FRB samples with different instruments ($10^{-10} - 10^{-7}$, Nicastro et al. (2021)) and only approaches the ratios expected from theory (10^{-6} Lyubarsky (2014) to 10^{-5} Metzger et al. (2019); Yang & Zhang (2021)). However, one should keep in mind that intrinsic fluence ratios may be significantly different from the observed ones due to beaming effects and that we need statistical limits on fluence ratio of lots of FRBs to constrain the models.

Unfortunately, the extragalactic distances and the expected faintness of FRB counterparts put them below the detection thresholds of currently available telescopes, observing at frequencies above the radio band. The nearest and brightest FRBs are the most promising candidates for multi-wavelength observations that could strongly

² https://heasarc.gsfc.nasa.gov/FTP/swift/data/obs/2017_10/00780203000/bat/rate constrain FRB emission models as the models become more quan-

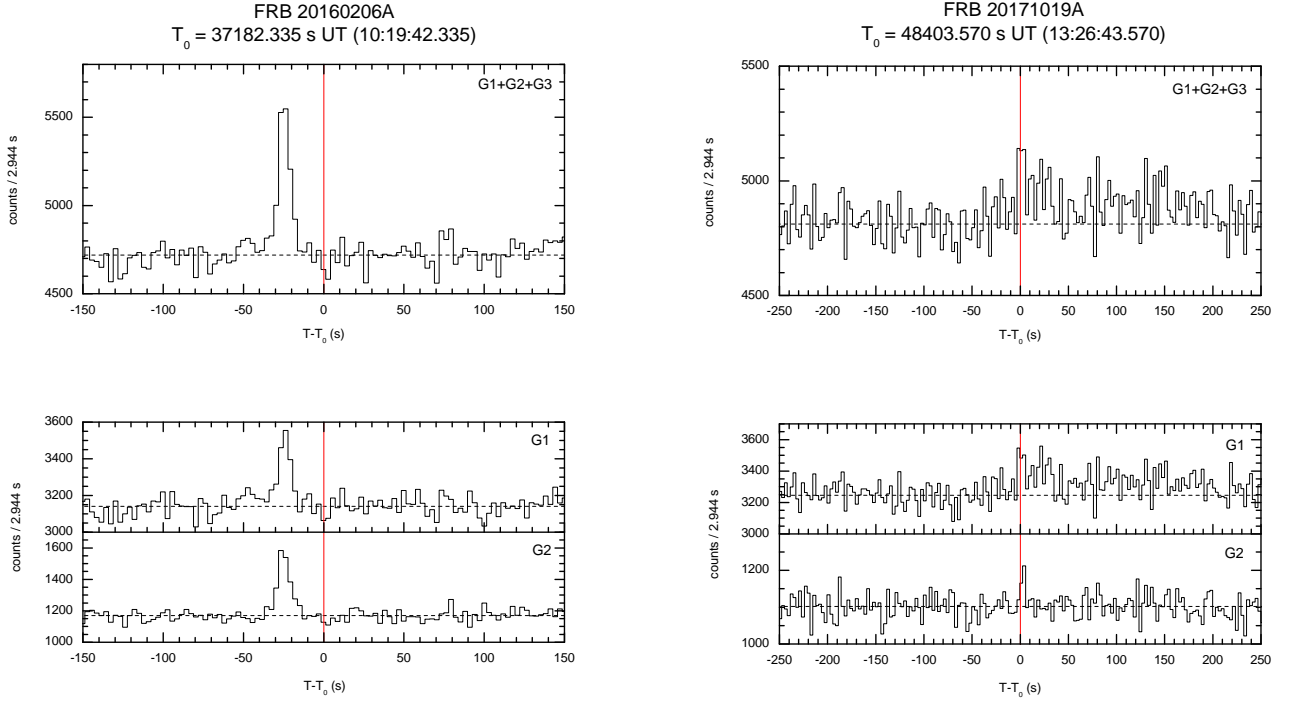


Figure 3. Candidate transient sources found for FRB 160206A (12σ significance, left) and FRB 171019A (5.3σ significance, right). Arrival time of FRBs corrected for delays due to dispersion and propagation marked by red line.

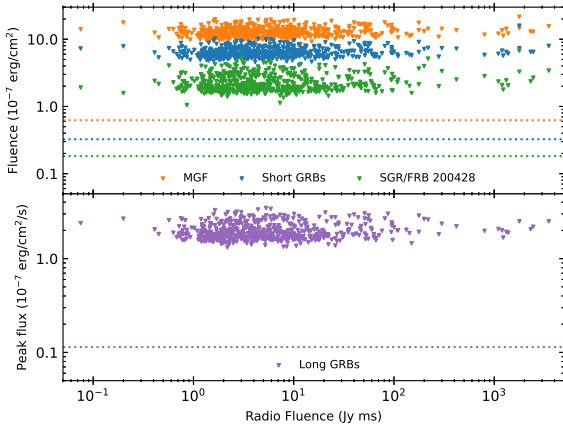


Figure 4. KW upper bounds on the 20-1500 keV fluence (top panel) for a short bursts having typical KW short GRB/MGF/FRB 200428 spectrum and on peak flux (bottom panel) of long bursts derived for 581 FRBs from our sample. The dotted lines show the results of the stacking analysis of non-repeating FRBs.

tative. At present, only two extragalactic FRBs are located in a relative proximity to us, i.e., FRB 181030A from a star-forming spiral galaxy NGC 3252 at a distance of 20 Mpc (Bhardwaj et al. 2021) and FRB 200120E from a globular cluster in M81 at 3.6 Mpc (Kirsten et al. 2022). From the stacked data analysis of nine bursts from FRB 181030A and six bursts from FRB 200120E in our sample, we derive the most stringent upper bounds on $E_{\text{iso}} \leq 6.5 \times 10^{45}$ erg and

Table 5. Radio fluences for non-repeating FRBs with measured redshifts.

FRB	Fluence (Jy ms)	Instrument	Cent. frequency (MHz)	Bandwidth (MHz)
180924B ^a	16 ± 1	ASKAP	1320	336
181112A ^b	26 ± 3	ASKAP	1295	336
190102C ^c	14 ± 1	ASKAP	1295	336
190523A ^d	≥ 280	DSA-10	1411	152.6
190608B ^c	26 ± 4	ASKAP	1295	336
190611B ^c	10 ± 2	ASKAP	1295	336
190614D ^e	0.62 ± 0.07	VLA	1400	1024
190714A ^f	8 ± 2	ASKAP	1272.5	336
191001A ^g	143 ± 15	ASKAP	920.5	336
191228A ^h	40^{+50}_{-10}	ASKAP	1272.5	336
200430A ⁱ	35 ± 4	ASKAP	864.5	336
200906A ^j	59^{+25}_{-10}	ASKAP	864.5	336

^a Bannister et al. (2019) ^b Prochaska et al. (2019) ^c Macquart et al. (2020) ^d Ravi et al. (2019) ^e Law et al. (2020) ^f Bhandari et al. (2019) ^g Shannon et al. (2019a) ^h Shannon et al. (2019b) ⁱ Kumar et al. (2020) ^j Bhandari et al. (2022)

$E_{\text{iso}} \leq 2.0 \times 10^{44}$ erg for short bursts from FRB 181030A and FRB 200120E, respectively.

Based on the bounds obtained from our observations, we can exclude GRBs with $E_{\text{iso}} \geq 7 \times 10^{50}$ erg, that are the majority of the observed by KW population ($\sim 97\%$; Tsvetkova et al. 2017, 2021), as counterpart candidates of localized FRBs from our sample. A magnetar flare origin of FRBs is consistent with the derived bounds in terms of either gamma-ray energetics, or radio-to-gamma-ray fluence ratios. For almost all FRBs considered, we can not rule out the occurrence of an extragalactic MGF, with isotropic energy similar

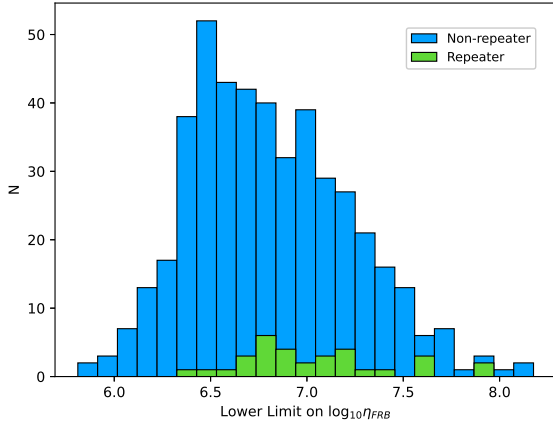


Figure 5. Lower bounds on the radio-to-gamma-ray fluence ratio distribution of FRBs with radio fluences measured by CHIME/FRB. The bounds are in units of $\text{Jy ms erg}^{-1} \text{cm}^2$.

to or smaller than that of GRB 200415A ($E_{\text{iso}} \sim 1.3 \times 10^{46}$ erg) or GRB 051103 ($E_{\text{iso}} \sim 5.3 \times 10^{46}$ erg) (Svinkin et al. 2021). MGFs with radio-to-gamma-ray fluence ratio similar to that of the 2004 giant flare from the Galactic magnetar SGR 1806-20 ($\eta_{\text{GF}} < 10^7$ $\text{Jy ms erg}^{-1} \text{cm}^2$; Tendulkar et al. 2016) are partly consistent with $\eta_{\text{FRB}} \geq 10^6 - 10^8$ $\text{Jy ms erg}^{-1} \text{cm}^2$ derived in this paper. The SGR/FRB 200428 event having a radio-to-gamma-ray fluence ratio of $\sim 7 \times 10^{11}$ $\text{Jy ms erg}^{-1} \text{cm}^2$ ($\sim 10^{-5}$ in dimensionless units) (CHIME/FRB Collaboration et al. 2020; Ridnaia et al. 2021) is far above our lower bounds on radio-to-gamma-ray fluence ratio. The most stringent KW bounds are placed using the stacked data analysis of bursts from two nearest FRB repeaters, these bounds rule out MGFs, but do not rule out short magnetar bursts with the typical emitted energies below 10^{42} erg.

Both detections and non-detections of FRB counterparts in multi-wavelength and multi-messenger search campaigns are of great importance. As in the case of other transient phenomena, for example, GRBs, collecting observational data at as wide as possible energy band are crucial for progress towards our understanding of these enigmatic events. The search of high-energy FRB counterparts with KW is a work in progress. With the rapid growth of FRB population we will soon be able to study several more close-by sources, and hence, significantly tighten bounds reported here.

ACKNOWLEDGEMENTS

The authors acknowledge support from the Russian Science Foundation (RNF) grant 21-12-00250.

DATA AVAILABILITY

KW data underlying this article will be shared from the corresponding author upon reasonable request. All the information of the FRB events in our sample together with the upper bounds on their high energy emission obtained in our analysis are available at the webpage <http://www.ioffe.ru/LEA/FRB/>. An example of tables provided online is given in the appendix.

REFERENCES

- Andersen B. C., et al., 2023, *ApJ*, 947, 83
- Anumarlapudi A., Bhalerao V., Tendulkar S. P., Balasubramanian A., 2020, *ApJ*, 888, 40
- Aptekar R. L., et al., 1995, *SSRv*, 71, 265
- Band D., et al., 1993, *ApJ*, 413, 281
- Bannister K. W., et al., 2019, *Science*, 365, 565
- Beloborodov A. M., 2017, *ApJ*, 843, L26
- Beloborodov A. M., 2020, *ApJ*, 896, 142
- Bhandari S., Kumar P., Shannon R. M., Macquart J. P., 2019, *The Astronomer's Telegram*, 12940, 1
- Bhandari S., et al., 2020, *ApJ*, 895, L37
- Bhandari S., et al., 2022, *AJ*, 163, 69
- Bhardwaj M., et al., 2021, *ApJ*, 919, L24
- Bochenek C. D., Ravi V., Belov K. V., Hallinan G., Kocz J., Kulkarni S. R., McKenna D. L., 2020, *Nature*, 587, 59
- CHIME/FRB Collaboration et al., 2018, *ApJ*, 863, 48
- CHIME/FRB Collaboration et al., 2020, *Nature*, 587, 54
- CHIME/FRB Collaboration et al., 2021, *ApJS*, 257, 59
- Chatterjee S., et al., 2017, *Nature*, 541, 58
- Chen G., Ravi V., Lu W., 2020, *ApJ*, 897, 146
- Cooper A. J., Wijers R. A. M. J., 2021, *MNRAS*, 508, L32
- Cordes J. M., Chatterjee S., 2019, *ARA&A*, 57, 417
- Cordes J. M., et al., 2006, *ApJ*, 637, 446
- Cunningham V., et al., 2019, *ApJ*, 879, 40
- Dong F. A., Chime/Frb Collaboration 2022, *The Astronomer's Telegram*, 15681, 1
- Fonseca E., et al., 2020, *ApJ*, 891, L6
- Frederiks D., Ridnaia A., Svinkin D., Lysenko A., Ulanov M., Tsvetkova A., 2022, *The Astronomer's Telegram*, 15686, 1
- Guidorzi C., et al., 2020, *Astron. Astrophys.*, 637, A69
- Heintz K. E., et al., 2020, *ApJ*, 903, 152
- Hotan A. W., et al., 2021, *Publ. Astron. Soc. Australia*, 38, e009
- Huang Y. X., et al., 2022, *The Astronomer's Telegram*, 15707, 1
- Kashyap V. L., van Dyk D. A., Connors A., Freeman P. E., Siemiginowska A., Xu J., Zezas A., 2010, *ApJ*, 719, 900
- Katz J. I., 2014, *Phys. Rev. D*, 89, 103009
- Kirsten F., et al., 2022, *Nature*, 602, 585
- Kozlova A. V., Svinkin D. S., Lysenko A. L., Ulanov M. V., Tsvetkova A. E., Frederiks D. D., 2019, in *Journal of Physics Conference Series*. p. 022014, doi:10.1088/1742-6596/1400/2/022014
- Kumar P., Lu W., Bhattacharya M., 2017, *MNRAS*, 468, 2726
- Kumar P., Day C. K., Shannon R. M., Bhandari S., Qiu H., Askap-Craft Collaboration 2020, *The Astronomer's Telegram*, 13694, 1
- Law C. J., et al., 2020, *ApJ*, 899, 161
- Li C. K., et al., 2021, *Nat. Astron.*, 5, 378
- Li X. B., et al., 2022, *The Astronomer's Telegram*, 15708, 1
- Lorimer D. R., Bailes M., McLaughlin M. A., Narkevic D. J., Crawford F., 2007, *Science*, 318, 777
- Lu W., Kumar P., Zhang B., 2020, *MNRAS*, 498, 1397
- Lyubarsky Y., 2014, *MNRAS*, 442, L9
- Maan Y., Leeuwen J. v., Straal S., Pastor-Marazuela I., 2022, *The Astronomer's Telegram*, 15697, 1
- Macquart J.-P., et al., 2010, *Publ. Astron. Soc. Australia*, 27, 272
- Macquart J. P., et al., 2020, *Nature*, 581, 391
- Martone R., et al., 2019, *Astron. Astrophys.*, 631, A62
- Mereghetti S., et al., 2020, *ApJ*, 898, L29
- Mereghetti S., Topinka M., Rigoselli M., Götz D., 2021, *ApJ*, 921, L3
- Metzger B. D., Margalit B., Sironi L., 2019, *MNRAS*, 485, 4091
- Mills B. Y., 1981, *Publ. Astron. Soc. Australia*, 4, 156
- Nan R., et al., 2011, *International Journal of Modern Physics D*, 20, 989
- Nicastro L., Guidorzi C., Palazzi E., Zampieri L., Turatto M., Gardini A., 2021, *Universe*, 7, 76
- Oosterloo T., Verheijen M. A. W., van Cappellen W., Bakker L., Heald G., Ivashina M., 2009, in *Wide Field Astronomy & Technology for the Square Kilometre Array*. p. 70 (arXiv:0912.0093), doi:10.22323/1.132.0070
- Perley R. A., Chandler C. J., Butler B. J., Wrobel J. M., 2011, *ApJ*, 739, L1

- Petroff E., Hessels J. W. T., Lorimer D. R., 2022, *A&ARv*, **30**, 2
- Platts E., Weltman A., Walters A., Tendulkar S. P., Gordin J. E. B., Kandhai S., 2019, *Phys. Rep.*, **821**, 1
- Popov S. B., Postnov K. A., 2010, in Harutyunian H. A., Mickaelian A. M., Terzian Y., eds, *Evolution of Cosmic Objects through their Physical Activity*, pp 129–132 ([arXiv:0710.2006](https://arxiv.org/abs/0710.2006)), doi:10.48550/arXiv.0710.2006
- Prandoni I., et al., 2017, *A&A*, **608**, A40
- Prestage R. M., Constantikes K. T., Hunter T. R., King L. J., Lacasse R. J., Lockman F. J., Norrod R. D., 2009, *IEEE Proceedings*, **97**, 1382
- Principe G., Di Venere L., Negro M., Di Lalla N., Omodei N., Di Tria R., Mazziotta M. N., Longo F., 2023, *A&A*, **675**, A99
- Prochaska J. X., et al., 2019, *Science*, **366**, 231
- Ravi V., DSA-110 Collaboration 2023, in *American Astronomical Society Meeting Abstracts*, p. 239.01
- Ravi V., et al., 2019, *Nature*, **572**, 352
- Ridnaia A., Svinkin D., Frederiks D., 2020, *J. Phys. Conf. Ser.*, **1697**, 012030
- Ridnaia A., et al., 2021, *Nat. Astron.*, **5**, 372
- Robertson J. G., 1991, *Australian Journal of Physics*, **44**, 729
- Shannon R. M., Kumar P., Bhandari S., Macquart J. P., 2019a, *The Astronomer’s Telegram*, **13166**, 1
- Shannon R. M., Day C., Kumar P., Askap-Craft Collaboration 2019b, *The Astronomer’s Telegram*, **13376**, 1
- Spitler L. G., et al., 2016, *Nature*, **531**, 202
- Staveley-Smith L., et al., 1996, *Publ. Astron. Soc. Australia*, **13**, 243
- Svinkin D. S., et al., 2016, *ApJSS*, **224**, 10
- Svinkin D., et al., 2019, *J. Phys. Conf. Ser.*, **1400**, 022010
- Svinkin D., et al., 2021, *Nature*, **589**, 211
- Svinkin D. S., et al., 2022, *ApJS*, **259**, 34
- Swarup G., Ananthakrishnan S., Kapahi V. K., Rao A. P., Subrahmanya C. R., Kulkarni V. K., 1991, *Current Science*, **60**, 95
- Tavani M., et al., 2021, *Nat. Astron.*, **5**, 401
- Tendulkar S. P., Kaspi V. M., Patel C., 2016, *ApJ*, **827**, 59
- Trudu M., et al., 2023, *A&A*, **676**, A17
- Tsvetkova A., et al., 2017, *ApJ*, **850**, 161
- Tsvetkova A., et al., 2021, *ApJ*, **908**, 83
- Tyul’bashev S. A., Tyul’basheva G. E., Kitaeva M. A., 2022, in *The Multifaceted Universe: Theory and Observations - 2022*, p. 43 ([arXiv:2208.04578](https://arxiv.org/abs/2208.04578)), doi:10.48550/arXiv.2208.04578
- Verrecchia F., et al., 2021, *ApJ*, **915**, 102
- Wang C. W., et al., 2022, *The Astronomer’s Telegram*, **15682**, 1
- Wielebinski R., Junkes N., Grahl B. H., 2011, *Journal of Astronomical History and Heritage*, **14**, 3
- Yang Y.-P., Zhang B., 2021, *ApJ*, **919**, 89
- Zhang B., 2020, *Nature*, **587**, 45

APPENDIX A: FRB DATA TABLES

The appendix gives an example of the FRB data tables, which can be found in full, machine-readable format online.

Table A1. Properties of the bursts from FRB 20200120E

FRB	Day (yyyymmdd)	Arrival Time UTC	RA deg	Dec deg	RA _{err}	Dec _{err}	DM pc cm ⁻³	DM _{err}	Facility	Freq. MHz	bandwidth MHz	RFluence Jy ms	PDelay s	DDelay s	KW Time UTC	UB _{SGRB} erg cm ⁻²	UB _{LGRB} erg cm ⁻² s ⁻¹	UB _{MGF} erg cm ⁻²	UB _{SGR} erg cm ⁻²
20200120E	20200120	35856.006	146.25	68.77	0.533	1.567	88.96	1.62	CHIME	600	400	-	3.272	1.0253	35858.253	5.44E-07	1.68E-07	1.08E-06	1.87E-07
20200718A	20200718	79951.867	149.1	68.79	0.600	1.433	88.96	1.62	CHIME	600	400	-	-3.405	1.0253	79947.437	5.04E-07	1.59E-07	9.94E-07	1.78E-07
20201129A	20201129	48689.858	149.43	68.77	0.483	1.283	87.75	0.4	CHIME	600	400	2.4	2.479	1.0113	48691.325	6.22E-07	1.94E-07	1.26E-06	2.38E-07
20210423G	20210423	13714.726	149.43	68.77	-	-	87.75	0.4	CHIME	600	400	-	0.547	1.0113	13714.261	6.15E-07	1.65E-07	1.22E-06	1.71E-07
20210430G	20210430	11942.401	149.43	68.77	-	-	87.75	0.4	CHIME	600	400	-	-0.077	1.0113	11941.313	4.63E-07	1.55E-07	9.17E-07	1.72E-07
20210823C	20210823	71036.557	149.43	68.77	-	-	87.75	0.4	CHIME	600	400	1.4	-3.499	1.0113	71032.047	5.52E-07	1.70E-07	1.14E-06	1.86E-07